Lunar megaregolith mixing by impacts: spatial diffusion of basin melt and its implications for sample interpretation

Tiantian Liu[a,b], Greg Michael[b], Kai Wünnemann[b,c], Harry Becker[b], Jürgen Oberst[a,d]

[a] Institute of Geodesy and Geoinformation Science, Technische Universität Berlin, 10623 Berlin, Germany (tiantian.liu@tu-berlin.de)

[b] Freie Universität Berlin, Malteserstr., 74-100, 12249 Berlin, Germany

[c] Museum für Naturkunde, Leibniz Institute for Evolution and Biodiversity Science, 10115 Berlin, Germany

[d] Institute of Planetary Research, German Aerospace Center (DLR), 12489 Berlin, Germany

Key Words

Moon, surface; Regoliths; Impact processes; Cratering

Abstract

The formation ages of lunar impact basins are critical to understanding the late accretion history of the inner solar system. Furthermore, the correct interpretation of the provenance and isotopic dates of basin-derived impact melt ('basin melt') is essential for the calibration of lunar chronology function. However, abundances of basin melt in the lunar near-surface are not well understood. Basin melt has been gardened by a long sequence of subsequent impact events, altering its abundance and size distribution. We developed a numerical model to investigate this process by means of the Monte Carlo method in a spatially resolved model. The fraction of melt in ejecta was tracked globally and at the Apollo 14-17 and Luna 20 sampling sites and was compared with K-Ar age distributions of lunar impact melt breccias. It was found that melt produced by the very large SPA basin as well as the relatively late-forming Imbrium basin should be dominant in the near-surface (top one meter). The simulation shows that the melt component at the Apollo 14-17 and Luna 20 sites is strongly affected by nearby mid- to late-forming basins. Imbrium melt should be abundant in Apollo 14-17 samples; Crisium melt is the most significant component of basin-sourced melt in Luna 20 samples; all the Apollo 14-17 and Luna 20 samples could include melt from Serenitatis and the SPA basin; Nectaris melt should occur in Apollo 16, Apollo 17 and Luna 20 samples; and Orientale melt has no significant mixing in the Apollo 14-17 and Luna 20 sampling sites. In general, besides a prominent age peak at 3.9 Ga (related to the Imbrium basin), the model predicts pronounced abundance peaks of older basin melt (>3.9 Ga) which tend to be absent from distributions of K-Ar ages of impactites from landing sites. The diffusion characteristics of basin melt suggest that for future sampling aimed at collecting early basin melt, the re-excavation zones of late impact craters larger than tens of kilometer in diameter inside basins may provide the highest abundances of melt from early basins.

1 Introduction

The lunar surface preserves a record of impacts in the inner solar system. Having a rigid crust and no atmosphere, its crater population is the best preserved among the solar system's planetary bodies, providing an essential record of late accretion in the inner solar system. Nevertheless, knowledge of the impact rate between 4.5 and 3.7 Ga, which may be related to different impactor populations, remains contested. Based on radioisotope ages (U-Pb system) of lunar samples that show clustered ages at ~3.9 Ga, Tera et al. (1974) suggested that there may have been an impact spike in the early lunar history ('lunar cataclysm'). This hypothesis was later further substantiated after larger numbers of K-Ar ages on impact rocks became available (Fernandes et al. 2013; Michael et al. 2018). The Nice model (Gomes et al. 2005; Morbidelli et al. 2012), which suggested that late migration of the giant planets could have destabilized part of the asteroid belt injecting projectiles into the inner solar system, was developed as a possible mechanism that might explain the occurrence of an impact spike. In contrast, based on studies of crater size-frequency distributions of surfaces in basins, Neukum (1983) and Hartmann (1995) argued that the Moon was hit only by one impactor population (the collisional remnants of planetesimals). In their view, the impact flux decayed monotonically and the dominant isotope ages of ~3.9 Ga just reflect sampling bias caused by the mixing of Imbrium ejecta.

The lunar basins can be used to constrain the impact rate in its early history if their ages are known. All lunar basins, including the youngest Orientale basin, formed before ~3.8 Ga by hypervelocity impact events. If the age of melt rocks that originate from a particular basin event can be determined reliably (e.g., by the K-Ar or other chronometers), it provides a calibration point for the lunar cratering chronology (Hiesinger and Head 2006). Basin melt also provides information on the regional chemical makeup of the crust, possibly providing clues to the lunar differentiation history. In addition, determining the distribution of basin melt is significant for lunar exploration, being a prime target for future robotic or human sample return missions (Ryder et al. 1989).

Melt from a specific basin is affected by the long-term gardening processes by later impact events. Its volume and composition is changed by re-melting, and its spatial distribution is altered by entrainment in younger ejecta materials (Michael et al. 2018; Liu et al. 2019, the characteristics of melt evolving distribution are described in supplementary section 2). The lunar meteorites and the lunar highland rocks collected by the Apollo and Luna missions have provided some information on the abundance of impact melt both in an average sense and at specific sites. However, there remains a considerable level of ambiguity in the interpretation of the origin of lunar meteorites and returned samples (Spudis et al. 2011).

In this study, we developed a numerical model to investigate the diffusion of basin melt by impact gardening. We use "diffusion" to describe the movement of impact melt down its concentration gradient by repeated impact events. The aim is to provide a picture of the potential distribution of basin melt by using a new modeling approach, and thus provide clues for the interpretation of returned samples regarding which age distributions of basin melt should be expected at previous and future landing sites. These data may also be used to assess interpretations of isotopic age distributions in the literature and in future studies.

In section 2, we present the structure of the model. In section 3, the melt component in the near-surface both on a global scale and at specific sampling sites is estimated and compared with distribution patterns of K-Ar ages. The spatial distribution of melt from three mid- to late- basins (Serenitatis, Crisium and Imbrium) in variable proximity to lunar landing sites is also examined. In section 4, we describe the implications for the interpretation of collected lunar samples and discuss sources of uncertainties in the model.

2 The Model

This paper is the third in a series investigating the cumulative melt diffusion by impact gardening. Michael et al. (2018) presented the surface-averaged model, where the volume of un-heated material and melt with different ages at different depth was traced. On this basis, Liu et al. (2019) investigated the diffusion behavior along a lateral path as well as by depth. Then, not only the distribution with depth, but also the lateral distribution along a path of a great circle was further recorded. This work extends the previous models, providing a more complete understanding of the melt evolving characteristics in three spatial dimensions, where the volume of unheated material and melt with different ages at all the depth over the global surface will be traced. We outline the main elements of the model here where we focus in particular on the new components of the model. Further detail is given in the Supplementary Material. In addition, in this model we do not consider the maria, because mare deposits cover parts of surface and occurred late, and hence would not significantly affect basin melt redistribution.

We used the Monte Carlo method to simulate the impact gardening process over the history of the observable surface of the Moon. The size-frequency distribution of generated craters conforms to the production function (PF) of Neukum (1983). The occurrence time of impacts was calculated combining the chronology function (CF) and PF (Neukum 1983). The minimum crater diameter considered was chosen as 5 km. The transient crater size, D_t, was calculated based on scaling laws (Melosh 1989; McKinnon et al. 1997). The volume of the generated melt markedly increases with D_t according to a power law (Cintala & Grieve 1998). The thicknesses of both ejecta and melt decrease with distance from crater center (r in km) following a power law, but the fraction (i.e. concentration) of melt in the ejecta linearly increases with distance (Liu et al. 2019; Melosh 1989). We note that our model considers the re-melting of the excavated material for individual impact events, but the possible resetting of the K-Ar clock in hot ejecta blankets was not incorporated because the detailed behavior of the K-Ar system in feldspars from impactites is poorly understood. (See Liu et al. 2019 and supplementary section 1 for details).

Materials ejected from craters have high kinetic energy resulting in mixing with local materials on re-impact. The degree of mixing is expected to increase with distance from the ejection point. We considered such local mixing in this new model. Oberbeck et al. (1975) proposed a mixing ratio of local material to ejecta, $\mu = 0.0183r^{0.87}$. However, these values, particularly at larger scales, were suggested to be overestimated in comparison with laboratory cratering experiments (Schultz & Gault 1985). The value of μ was thus modified by roughly half when μ is larger than 5.0: $\mu' = \mu/2 + 2.5$ (Petro & Pieters 2006).

The model used point sets on a sphere to record the material component. The locations of these points were calculated based on the Fibonacci Lattice (González 2010) to make them uniformly distributed on the surface. Each point was related to a cell. For each impact event, the points within tracing ranges (five radii of transient craters) will be found first. In each of these points, the melt volume, the total volume including both melt and un-melted component, and the thickness of ejecta (and melt lens within craters) will be recorded. When projecting the point set onto a plane, we used a Voronoi diagram (i.e. Thiessen polygon) to represent the cell of each point.

Because of the increasing number of deposition layers as the simulation progresses, the layer sequence was periodically simplified to one: 0.2×1.9^{a} m, where a = 0, 1, …, 20. While simplifying, all the material within set layers will be mixed together leading to a more average composition. The shallower layers are thinner to preserve a fine resolution of the melt component in the near surface; deeper layers are thicker yielding a more averaged composition.

3 Results

Lunar meteorites and the immediate source of current lunar samples are from the near-surface down to a few or tens of meters. Understanding the source and age distribution of the melt component in the surface layer is critical to our understanding of the lunar chronology, and key in the selection of future sampling sites. This study therefore focuses on the distribution of impact melt in the near-surface (top one meter).

3.1 Timing of basin-forming events

To investigate the melt distribution of the lunar impact basins, a model was created using both the known sizes and positions of the basins and randomly distributed craters smaller than 300 km. Thirty basin-forming events, the crater populations of which were reinvestigated using the buffered non-sparseness correction technique, are included in our simulations (Orgel et al. 2018). The buffered non-sparseness correction technique takes crater obliteration into account for the superposed crater densities, providing more accurate measurements of the occurrence times of basins (Riedel et al. 2018). Neukum et al. (2015) present a more complete list of lunar basins where some potential large lunar basins, such as Aestuum, Lamont, and Hertzsprung basins, are not included in the list in Orgel et al. (2018). The occurrence times of these basins, however, have not been calculated. They are therefore not included in this model. The erased structures of these basins indicate their early formation times. The consequences of excluding these basins are discussed in section 3.3.

Since the scaling laws used to calculate transient crater diameter (D_t, supplementary section 1) do not extrapolate well to basin sizes, we adopt the D_t values of 11 basins from Wieczorek & Phillips (1999) where the transient basin size was determined using gravity models. The D_t of the other basins was interpolated. The locations of the basins showing D_t and age is presented in Figure 1, and Table S1 presents the age, location and size of all the included basins.

It should be mentioned that the formation times of basins included in the simulations are taken as a plausible configuration of impact times, and are not claimed as being in any way 'well known'. Our goal is to address the question "What are the consequences of such a configuration of impacts for the sample record?" and to use the comparison with the actual record of isotopic ages to inform our understanding of both the period and the process of basin melt migration into lunar impactite samples. The influence of an alternative sequence of basins will be discussed in section 4.3.

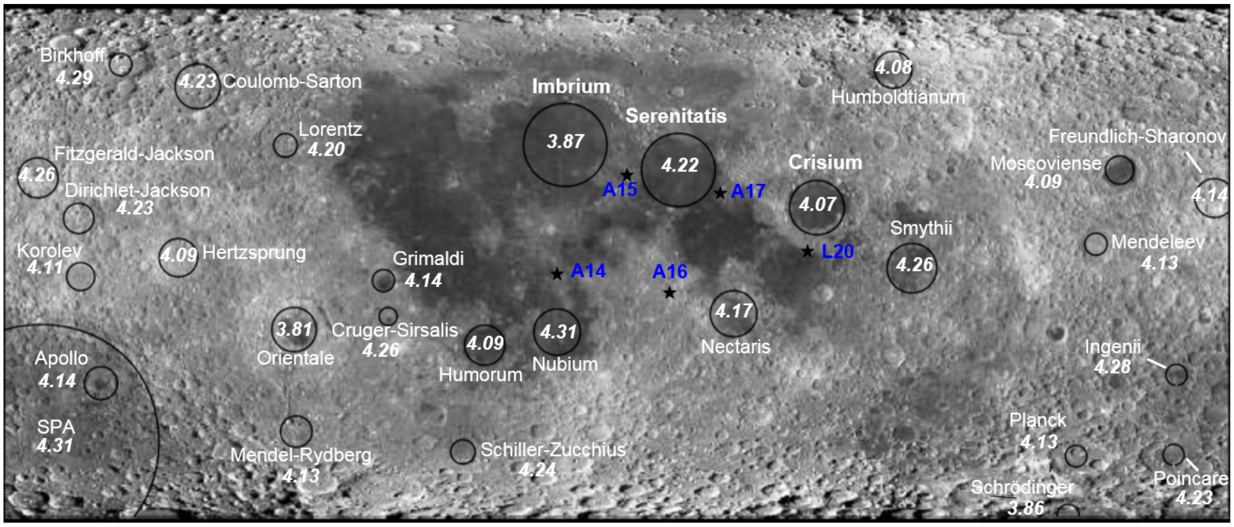

Figure 1 Map of basins. Circles mark the estimated transient cavities of 30 basins, and the numbers indicate their estimated ages (Orgel et al. 2018). Filled stars mark the locations of Apollo 14-17 (A14-17) and Luna 20 (L20) sampling sites. The background image is Lunar Reconnaissance Orbiter Camera (LROC) Wide Angle Camera (WAC) mosaic (<75° in latitude) (Robinson et al. 2010). The ages are based on recent work by Orgel et al. (2018).

Simulated impacts start slightly before the estimated formation time of the SPA basin at 4.31 Ga. In one simulation run there were 162517 impact events in total, including basin-forming events. Many older impacts have no significant influence on the present near-surface, since the majority of their melt was buried deeply by the ejecta of younger impacts. We improved the efficiency of the model by filtering out those impacts which we are certain to have negligible contributions to the near-surface melt abundance (the filtering procedure is described in supplementary section 3). After the filtering, 29176 impacts remain, while 133341 have been removed. As a consequence, the time for one run is decreased from five days to four hours. Of those removed, 96.9% are smaller than 30 km. Because of the greater impact flux during the early period, the majority of craters filtered out were old (Figure S 4b), with 99.97 % being older than 3.5 Ga. The difference of the relative expected melt component at different depths is smaller than ~0.02, indicating that the features of melt component distribution are well-preserved by the filtering procedure.

3.2 Average melt component in the lunar near-surface layer

If lunar meteorites provide a spatially stochastic sample of lunar highland materials, the statistical radioisotope age record of melt-bearing impact rocks among lunar meteorites could reflect the average distribution of the melt component. We estimated the fraction of impact melt in the top one meter for comparison with the radioisotope age record (Figure 2).

The predicted distribution of melt with different ages is shown in Figure 2c. Basins are the main contributors of melt older than ~3.8 Ga. As indicated by the dashed arrows in Figure 2, the largest, SPA basin (~2500 km) is predicted to provide the most abundant melt in the near-surface; The late-forming Imbrium basin (~1320 km) is the second largest contributor of melt. Other basin events also left distinct traces: the melt of the youngest Orientale basin (3.81 Ga) is ~0.4× as abundant as Imbrium melt leading to the secondary peak at 3.81 Ga; several basins forming between 4.10 and 4.25 Ga generate a bulge during this period. To predict the contribution of basin-sourced melt, Table S2 presents volumes of melt from basins and smaller impacts. In general, younger basins leave more melt in the near-surface today.

We expect that there would have been basin-forming impacts prior to those which we are able to observe today (e.g., Neumann et al. 2015; Zhu et al. 2019). It can be expected that impacts occurring in the period between crustal solidification and the time of the presently observable oldest surfaces would leave a melt component, which could persist within the crust until now.

These early impact events would heat and alter more crust material and the generated melt ought to leave a trace from depth up to the surface until the present day (see Michael et al. 2018). We recognize, however, that this material could be highly comminuted by impact gardening and partially remelted by younger impacts near the surface, which may leave it unrecognizable there (see further discussion in section 4.1).

During the last 3.0 Ga, the impact rate was lower and remains constant, melt diffusion is thus generally constant and the melt production is much less. Such a lower impact rate leads to a lesser amount of older melt being re-melted. Therefore, in the near-surface, younger impacts leave comparable quantities of melt to older basins, as indicated by relatively large impacts seen as random peaks in Figure 2c, such as those at 0.4 and 3.3 Ga.

Fernandes et al. (2013) compiled published K-Ar data and calculated the relative probability of $^{40}Ar/^{39}Ar$ impact ages from lunar meteorites, where 65 samples were included and the age was corrected for monitor age and decay-constant. Their plot is shown in Figure 2b. It is seen that, in the radioisotope age record of impact melt breccias in lunar meteorites (Figure 2b), there is abundant melt older than 3.5 Ga as expected, but less than expected with ages >3.8 Ga. In addition, in the distribution of isotopic dates (Figure 2b), the presence of melt from later impact events is more significant. The possible cause of these differences will be discussed in section 4.1.

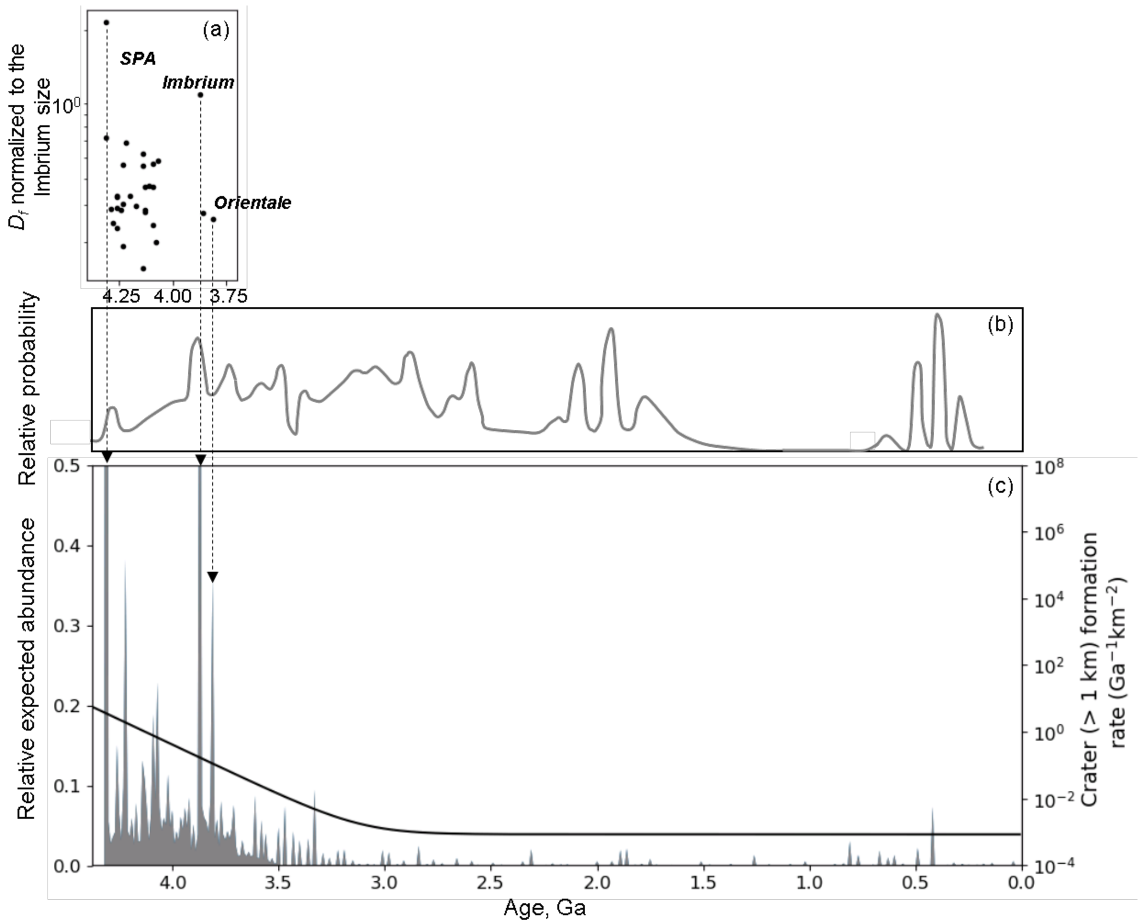

Figure 2 (a) Size distribution of basins normalized to the diameter of Imbrium basin. The formation times of SPA and Imbrium basin from Orgel et al. (2018) are $\mu 4.31^{+0.019}_{-0.021}$ $\mu 3.87^{+0.035}_{-0.046}$ Ga, respectively. (b) Relative probability plot of $^{40}Ar/^{39}Ar$ from 65 impact melt clasts in lunar meteorites (after Fernandes et al. 2013). The vertical scale is linear. The peak near 3.8 Ga is commonly interpreted to reflect the age of the Imbrium impact. (c) Fraction of melt component (i.e. relative melt abundance among all the generated melt) in the top one meter of lunar near-surface (left scale). The expected melt generated by SPA, Imbrium and Orientale basins are indicated by three vertical arrows. To show the small melt quantity from smaller impacts, melt fractions have been normalized to the absolute melt fraction derived from the second most abundant melt reservoir, the Imbrium basin (i.e. its relative abundance is equal to 1.0). The crater formation rate (right scale) shows that the high impact rate in the early lunar history is accompanied by a greater melt production. Note that if melt fractions were normalized to SPA melt fractions, the relative quantity of other melt fractions would be so small that specific distribution features are easily masked. Thus, the relative abundance of SPA melt fraction exceeds 1.0, and the exact value is not presented.

3.3 Present-day distribution of melt from basins formed between 4.2 and 3.8 Ga

Due to the weaker gardening after 3.0 Ga, abundant melt of basins formed between 4.2 and 3.8 Ga (mid- to late-forming basins) could survive in the near surface, and is thus very likely to be sampled. As representative examples, we present the global near-surface melt distribution of the Serenitatis, Crisium and Imbrium basins (Figure 3).

Besides the mare-related volcanism, which is not taken into account in this model, the only process that can significantly modify the distribution of basin melt is gardening by other basin-scale impact events. Smaller impact events can only re-melt small portions of older melt. Because nearly no disturbance by younger basin forming impacts occurred, Imbrium melt is well-preserved and predominant in the near surface (Figure 3a). Imbrium ejecta covered the northwest part of Crisium ejecta, decreasing the abundance of Crisium melt in the near surface. Serenitatis is located between the Imbrium and Crisium basins (Figure 1). The excavation zones of both the Imbrium and Crisium basin exhumed the earlier Serenitatis ejecta. In the model, both the Crisium and the Imbrium ejecta entrained Serenitatis melt, transporting it to more distant locations. Therefore, the coverage of Serenitatis melt is almost equal to the merged zone of both Crisium and Imbrium ejecta (the main coverage by Imbrium and Crisium melt is outlined by a dashed curve in Figure 3). Nevertheless, the quantity of entrained Serenitatis melt is low. The average melt fraction from Imbrium is about ten times larger than from Serenitatis and double that of Crisium.

Subsequent smaller impact events garden the basin melt locally, making the distribution patchy. They diminish or even remove the melt from the excavation zones. The fraction of the basin melt entrained in the ejecta of smaller impacts depends on their scale and location. If an impact event is large enough to excavate older basin melt, it can form melt-enriched zones in the near-surface, especially if it excavates melt from the basin interior or the melt near the rim of the basin. Two regions enriched in Serenitatis melt are indicated by the black arrows in Figure 3c. Most smaller impacts occur on the ejecta areas of basins, excavating only a limited amount of basin melt and distributing it further, slightly reducing the proportion of basin melt in the near-surface. These zones are shown as faded red and yellow in Figure 3a and b.

The results have some important implications for future sampling aimed at collecting the melt from these three basins. Within the range of several basin radii from Imbrium's center it is very likely to find its melt. Crisium melt could also be abundant, but will be mixed with that of Imbrium within the Imbrium ejecta field. To limit the influence from the Imbrium basin, it would be better to collect samples from the eastern part of Crisium basin. Sampling Serenitatis melt without an admixture from other basins is difficult. It is the most wide-spread, but due to its low probability of preservation at the surface, re-excavation zones may be the best candidates for samples possessing a higher fraction of its melt. It should be noted that, most of regions within the basins were flooded by mare basalts, but if impact events penetrated mare basalts and excavated underlying impact melt, this basin melt should be the most abundant component in the ejecta, besides mare basalt.

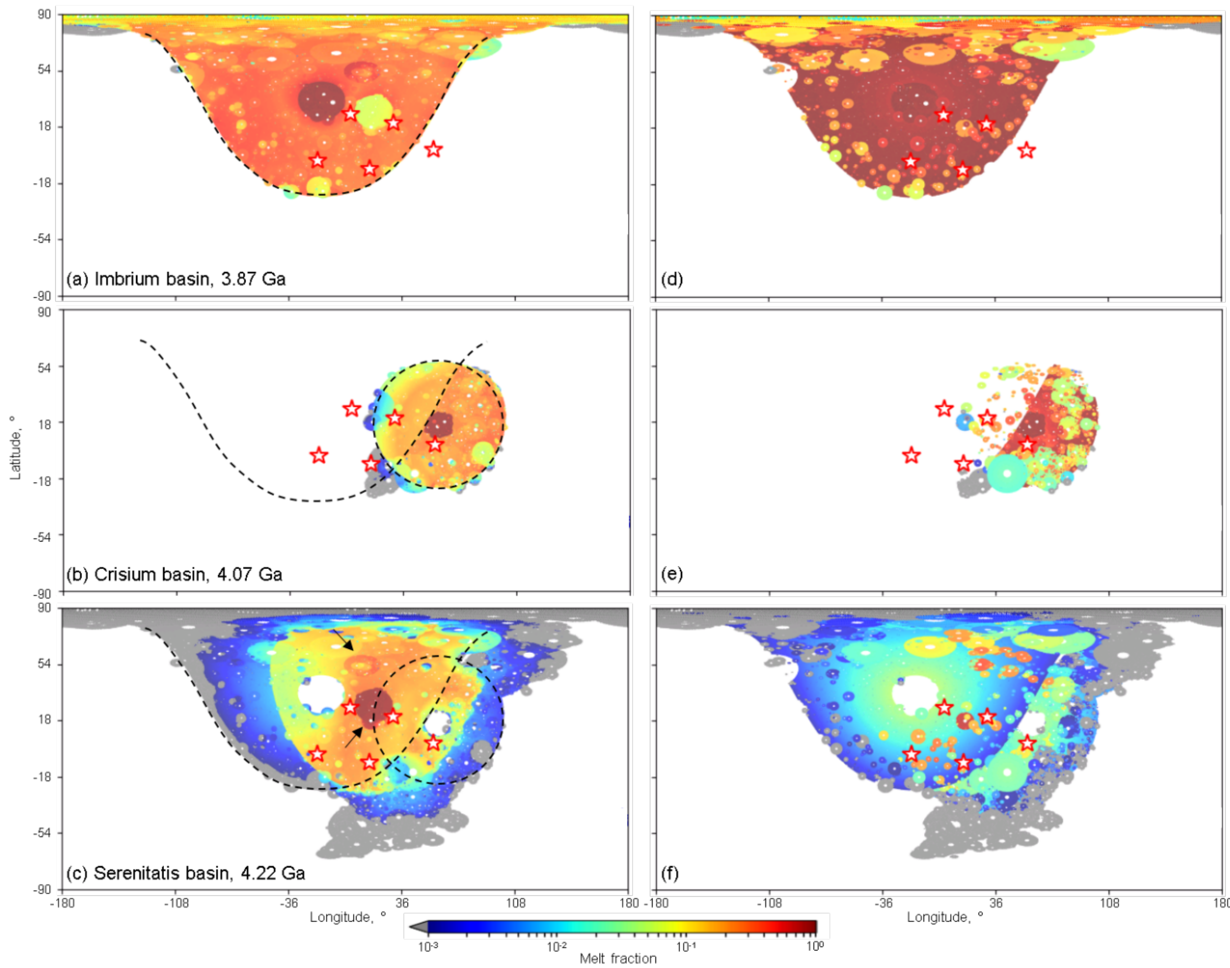

Figure 3 The global present-day distribution of melt from Imbrium (a), Crisium (b), and (c) Serenitatis basin in the near-surface (top five meters). Warmer colors indicate higher melt fractions (i.e. fraction of basin melt among all impact melt). Red stars indicate Apollo 14-17 and Luna 20 sampling sites. The main coverage of Imbrium and Crisium ejecta is indicated by the dashed regions. The black arrows in (c) indicate re-excavation zones of Serenitatis melt. (d)-(f) are the expected Imbrium, Crisium and Serenitatis melt abundances without local mixing processes.

3.4 Basin-sourced melt abundances at Apollo and Luna sampling sites

Without knowledge of their source, the context of lunar samples is difficult to evaluate. We calculated the probable fraction of basin-sourced melt in the near-surface at Apollo 14-17 and

Luna 20 landing sites. These simulation results can be helpful for the interpretation of sample data and radioisotope ages in future work (Figure 4a-e). The volumes of melt from basins and smaller impacts are shown in Table S3. Note that, since no mare basalt or other late volcanic deposits are taken into account in this study, the following discussions concerning the fractions of basin melt do not consider admixtures of mare basalt which were found to be abundant in some returned samples (e.g., Shervais et al. 1985).

The melt component at these sites is strongly influenced by the ejecta of the youngest and closest basin. As seen from Figure 3, the Apollo 14-17 sampling sites were covered by Imbrium ejecta, and the Luna 20 samples were extensively mixed with Crisium ejecta. Therefore, impact melt components in the Apollo 14-17 samples are expected to be dominated by Imbrium melt. The fraction of Imbrium melt is expected to be ~1.0 in the melt with ages of 3.87 Ga (Table S2), which is suggested by its high relative abundance at 3.87 Ga in Figure 4a-d highlighted by red color. Luna 20 samples would contain abundant Crisium melt with a fraction of 0.92 in the melt with an age of 4.07 Ga (Table S2), indicated by the pronounced peak with this age (Figure 4e) highlighted by green color. Since both Imbrium and Crisium excavated the older Serenitatis material, all the Apollo 14-17 and Luna 20 samples should be mixed with at least some Serenitatis melt. Although the volume is small, Serenitatis melt is still the major contributor in melt with an age of 4.22 Ga (Table S2). Traces of the nearby older basin events should also be found in impactites collected near the surface, but their contribution would be small due to dilution by the later events. For example, Nectaris melt could be found at the Apollo 16-17 and Luna 20 landing sites (4.17 Ga in Figure 4c), but its quantity is small. The melt of the youngest Orientale basin has no significant mixing in the Apollo 14-17 and Luna 20 sampling sites.

Not all large peaks in the melt age distribution were derived from basins. Younger melt generated by smaller impacts (i.e., non-basin) also leaves traces, as those younger melts have experienced less gardening. Taking Luna 20 as an example, according to its location, the high quantity of melt at 3.87 Ga (Figure 4e) is derived from smaller impacts at this time, rather than a basin forming event. For the Apollo 14 sampling site, the model predicts only the peaks at 4.31 Ga, 4.22 Ga, 4.10 Ga and 3.87 Ga to be caused by basin forming events. Smaller impacts are randomly distributed over the lunar surface, and thus the simulation will not exactly match what is found at a specific site. The expected peaks caused by younger impacts are therefore different from some sample ages. This might also be the case for the record from lunar meteorites (Figure 2, Fernandes et al. 2013).

Michael et al. (2018) aggregated 117 K-Ar age measurements of Apollo 14-17 and Luna 20 impact melt breccias in highland rocks. The relative probability of K-Ar ages is plotted above each histogram in Figure 4. By comparing the expected melt abundance with the distribution of K-Ar radioisotopic ages, the issue of whether the peaks displayed in the radioisotopic ages is related to the basin forming events could be further evaluated.

Note that the recently proposed age of the Imbrium basin derived from U-Pb dates of phosphates in breccias from the Apollo 14 landing site is 3.9±0.02 Ga (Snape et al., 2016). Crisium age was proposed to be 3.95-3.85 Ga (Stöffler 2006). The apparent age of the Imbrium basin (3.87 Ga) and Crisium basin (4.07 Ga) from crater size-frequency distribution (CSFD) and the Neukum (1983) chronology function, may be slightly inaccurate because of a combination of factors. Earlier decay constants used to calculate ^{40}K-^{40}Ar ages and ^{87}Rb-^{87}Sr ages during the 1970s and early 1980s are slightly different from recent determinations (Jourdan 2012; Naumenko-Dèzes et al. 2019; Rotenberg et al., 2012). Furthermore, uncertainties of ages of neutron fluence monitors used in Ar-Ar dating and uncritical use of data from disturbed isochrons and complex Ar release spectra are additional biases on presumed basin ages that use isotopic dates and such biases also affect age distributions such as Figure 2 and 4 (see Jourdan et al., 2009; Jourdan, 2012; Norman et al., 2010; Fernandes et al., 2013). In the following, we will use the 3.87 Ga age as representing the age of Imbrium, even though the true age may be 30-50 Ma older. The reasoning is that both age distributions (Figure 2 and 4) and the impactor flux and basin ages used as a basis for our model were affected by the biases mentioned above.

We note that all isotopic age distributions from landing sites of the present study reveal the Imbrium peak of 3.87 Ga. However, additional 'age' peaks near 3.87 Ga are also sometimes present and may either result from smaller impact events or may reflect the presence of disturbed age spectra in the distributions. Both the Apollo 17 and Luna 20 sampling sites are expected to possess abundant Crisium melt (green histograms of 4.07 Ga in Figure 4), but the distribution of radioisotope ages does not display the corresponding peaks, and only few ages occur near 4.1Ga. If the proposed Crisium age of 3.95-3.85 Ga is taken (Stöffler 2006), which is indicated by the semitransparent-green bars in Figure 4, the simulation results would be consistent with the radioisotopic dates shown as the peak of ~3.9 Ga. It may suggest that the melt of ~3.9 Ga in the Apollo 17 and Luna 20 samples could be mainly derived from the Crisium melt. If so, then the formation time of Crisium basin is more likely to be ~3.9 Ga which is close to the age of Imbrium basin, and the overlapping of semitransparent-red and green bars at ~3.9 Ga (Figure 4d) indicates that Apollo 17 samples may be a mixture of both Imbrium and Crisium melt.

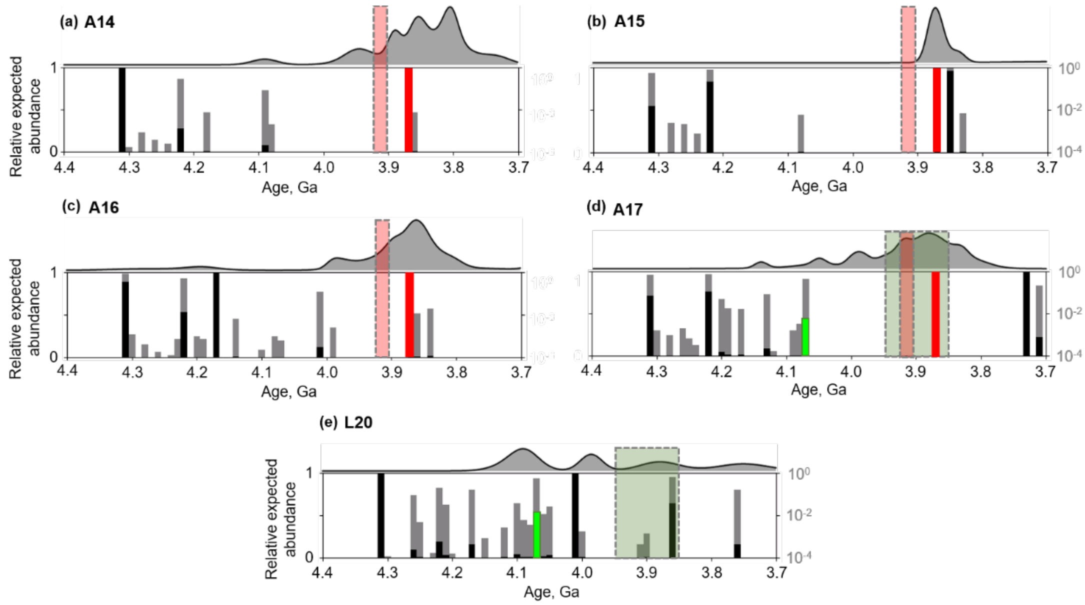

Figure 4 Relative distribution of K-Ar dates obtained on impact melt breccias at the Apollo 14-17 and Luna 20 sampling sites from samples (upper diagrams, Michael et al. 2018) in comparison with relative melt abundances at the Apollo 14-17 and Luna 20 sampling sites based on simulations (lower histograms; relative abundance among all the generated melt). The simulation data reflect melt abundances over a radius of 50 km at each landing site in the top 1 m of the near-surface. Model histograms are shown in black (absolute scale, left) and in grey (logarithmic scale, right). In the black histograms, the peaks caused by Imbrium (3.87 Ga) and Crisium (4.07 Ga) melt are highlighted by red and green color, respectively. Both ages were calculated based on the Neukum (1983) crater chronology and decay constants of that time, which are also the basis of the impactor flux used in our model (see text for further explanation). Note that Pb-Pb ages of phosphates suggest that the true age of the Imbrium basin is probably 3.92±0.02 Ga (the semitransparent-red bar, Snape et al., 2016). Stöffler (2006) suggested that Crisium-derived melt was 3.95-3.85 Ga (the semitransparent-green bars). Overall, the abundance of Imbrian 'ages' near 3.87 Ga at the Apollo landing sites agree with predictions from the model, whereas older K-Ar ages are much less common or do not occur (Apollo 15).

4 Discussion

4.1 Implications for the interpretation of melt provenance at lunar landing sites

The model predicts less young melt and more older melt (>~3.8 Ga) than implied by the K-Ar age distributions (Figure 2 and Figure 4). In addition, some of the expected peak values of melt abundance show different ages compared to the K-Ar age peaks. The main assumption in comparisons between age peaks in the model and published K-Ar ages is that the latter represents a statistical measure of the abundance of melt rock at the particular landing site and also globally. However, this assumption is not certain, and may be incorrect. A second assumption is that the model ages of basins are correct, but they could be inaccurate due to the inherent uncertainties in the lunar chronology function.

The radioisotope age distributions show prevalent younger melt rock. Many previous studies have investigated plausible causes of the apparent deficient of the old melt rock (e.g., Chapman et al. 2007; Cohen 2000; Hartmann 1975; Zellner 2017). It could be caused by the complete or partial Ar loss of older melt rocks and mineral clasts due to heating and shock, whereas inheritance of Ar from undigested older feldspar clasts in melt rocks might yield apparent ages that cannot be related to specific events (Korotev 1994; Norman et al. 2006; Norman & Nemchin 2014). Older clasts in melt breccias and their minerals may have been contaminated by younger (Imbrian) KREEP rich impact melt which may influence Ar budgets. In addition, older melt clasts may be less abundant than predicted because they were digested in large impact melt sheets or incorporated in warm ejecta blankets and all previously accumulated radiogenic Ar was lost because of degassing (Fernandes et al. 2013; Norman et al. 2006; Norman et al. 2010). Furthermore, as the grain size of melt rocks decreases with time due to gardening, older melt is more likely to survive near the surface in the form of tiny clasts or fine-grained minerals in breccia matrices. The larger clasts of melt rocks from younger basin forming impacts such as Imbrium may have been preferably chosen for dating, and thus young ages show up more frequently.

A significant number of published ^{40}Ar-^{39}Ar ages on lunar melt rocks or feldspars are based on perturbed age spectra, most of which do not satisfy current statistical tests for a point-like geological event (at least ~70% of the age spectrum (Cassata et al. 2009)). Such samples may yield apparent dates that are shifted towards younger or older dates by tens and even hundreds of millions of years. A review of the geochronology of impact melt breccias by Grange et al. (2010) suggests that, when using strict data filtering (Jourdan et al. 2009), only a few tens of $^{40}Ar/^{39}Ar$ data of almost 300 sample analyses yield well-behaved and reliable age spectra (e.g. $^{40}Ar/^{39}Ar$ plateau ages given by Norman et al. 2006, Norman et al. 2010, and Fernandez et al. 2013). A better understanding of the chronology of major basin-forming impacts would require a much more systematic study of a larger number of samples, both from existing collections and from sample sets brought back by future missions.

Although a comparison of detailed aspects of the age distributions with the model results are difficult (e.g. the number of recorded impact events or ages of specific basins, Niihara et al. 2019; Norman et al. 2006) some robust general features may help to advance interpretations in future studies. According to our results, basin ejecta from the late-formed Imbrium and also the Crisium basin, should be the most significant components which should show up in the distribution in the K-Ar ages. In case of Imbrium, K-Ar ages near 3.87 Ga are common and match the model (Figure 4). For Crisium, a model age of 4.07 Ga could reflect data from some Apollo landing sites, whereas data from Luna 20 (which is closer to Crisium than the Apollo landing sites and relatively far away from Imbrium) would be more supportive of a relatively young age (3.85-3.95 Ga; Stöffler 2006). Both the model of ejecta ages and isotope age distributions at landing sites may be affected by locally produced impact melt from small impacts (see Figure 2 and 4). Such biases may be evaluated by multi-chronometer studies of samples, combined with petrological and geochemical information. A key result of the data in Figure 4 is the absence (Apollo 15) or rarity of > 4.1 Ga old impact melt (i.e. melt from basins such as Serenitatis and South Pole Aitken) among isotope ages which is in contrast to the predicted minor abundance of such melt at the landing sites. As discussed above, this could reflect efficient loss of Ar from old melt clasts by younger heating events, biases during sampling of melt breccias, for instance if ancient melt rocks have a small grain size, or inaccuracies in our model.

4.2 Implications for future basin-melt targeted sampling

Linking the lunar samples to specific basins is a critical step in understanding the lunar history. Other than Imbrium, there is little consensus on which melt rocks or clasts retrieved from the Apollo and Luna missions were derived from specific basin events (Stöffler 2006).

Theoretically, the best locations to collect basin melt would be the basin floor where the majority of melt is deposited after basin formation. However, old basins were mostly later filled with mare basalt, burying the impact melt by up to several kilometers.

Later impacts that are larger than tens of kilometer in diameter with excavation depths of several kilometers are likely to penetrate the mare basalt cover and form regional domains enriched with older melt rocks. Such impact craters are even more promising when located near the basin rim, because of the higher melt abundance there. For example, although the majority of Serenitatis melt was buried, the model predicts that there are still some regions in the near-surface possessing a large fraction of Serenitatis melt as indicated by arrows in Figure 3c. The potential for excavation of deeper ejecta blankets by young impacts has been also discussed in geochronological and geochemical studies of impactites from the Apollo 16 landing site. For instance, recent data support arguments that the 50 Ma old North Ray Crater excavated deeper stratigraphic ejecta units that were mainly derived from the Imbrium impact (Norman et al. 2010; Norman et al. 2016). Clast proportions, age distributions and geochemical characteristics in the deep units are different from the more shallow Cayley Plains Formation in that area, which is also interpreted to be Imbrium-derived (Norman et al. 2010).

The SPA region is also one of hot targets of future lunar missions (e.g. oft-suggested MoonRise mission). Figure 5 presents the predicted melt composition inside the SPA cavity (top one meter). Among all the generated impact melt older than 3.8 Ga, the SPA melt could be far more than those of later-formed impact events. In addition to the SPA melt, impact melts of Pointcare and Apollo basins would be the most prominent components regarding to the giant-basin forming events. In addition, due to the high impact flux in the early history, the impact melt of smaller impact events could also leave significant abundance until now, which would make the interpretation of surface material difficult.

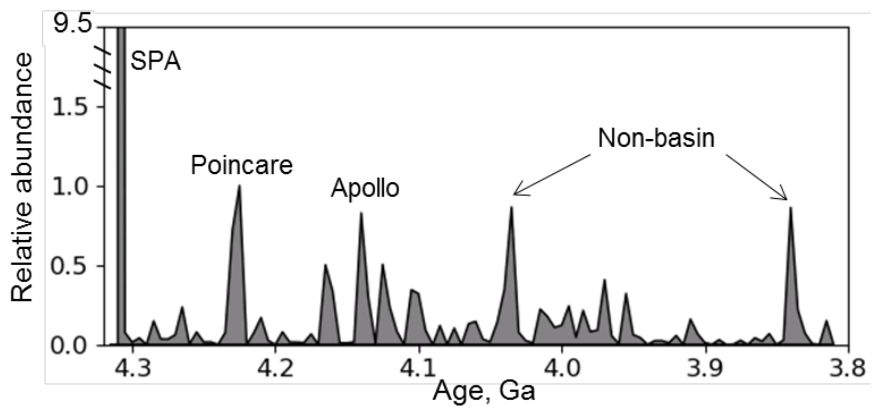

Figure 5 Predicted melt component in the top one meter within the SPA region.

4.3 Effects on model results of varying input parameters

To estimate the sensitivity of the model, here, we describe the effects of varying input parameters. For each tested parameter, we keep the other values as previously.

i) Melt produced in individual impacts

The scaling law applied to calculate the total volume of generated melt of individual impacts is derived from observations and numerical models for materials heated above melting point after release from shocked state (Cintala & Grieve 1998). However, the K-Ar closure temperature of feldspars is significantly lower than the solidus temperature of basic lunar rocks, although the applicability of the closure temperature concept in rapid heating and cooling processes during impacts is uncertain. Therefore, the term “melt” used here should be regarded as “hot ejecta” that include all material heated above the K-Ar closure temperature of lunar rocks (Liu et al. 2019). The total volume of “hot ejecta” could be greater than of the estimate for “melt”. To check its influence, simulations with slightly (two times) and significantly (ten times) more melt production in each impact were performed. We found that (Figure S5 in supplementary material), in the top 500 m, when the melt of individual impact is two times more, the difference of relative melt fraction is generally smaller than 0.05, which results in ~15% difference of melt fraction compared with the result shown in Figure 2. When the melt of individual impact is ten times more, in the top ten meters, the difference of relative melt fraction compared with the result shown in Figure 2 is generally smaller than 0.1; at greater depth, the difference is larger, but is generally smaller than 0.2 compared with the result shown in Figure 2. In both cases, however, old basin melt, predominantly remains in the near-surface: it is not erased by later events

ii) Ejected melt volume

Only a minor portion of the generated impact melt would be ejected outside the craters. In this model, 75% of generated melt stays within the crater, with 25% being ejected. Simulations with instead 20% and 30% ejected melt of individual impacts were performed. The results (Figure S6 in supplementary material) show that, in the top 500 m, the difference of relative melt fraction is <~0.02, which results in ~10% difference compared with the result shown in Figure 2a.

iii) Sequence of basins

Although the sequence of lunar basins is roughly known, some basins display inconsistent sequences based on different measurement techniques (Fassett et al. 2012; Orgel et al. 2018; Stöffler 2006). For example, in the past, the Nectaris basin was suggested to be older than Serenitatis basin, which contrasts with the results of Orgel et al. (2018). To test the influence of an alternative age sequence of basins, we assumed that Serenitatis formed after the Nectaris basin, the ages of other basins remaining unchanged. The simulation result shows that (Figure S7) the difference of the fraction of Serenitatis melt in the near surface in these different age models for Serenitatis and Nectaris is generally smaller than ~0.01. The major difference is the absent of Serenitatis melt surrounding the Nectaris basin since ejecta from the "early-formed" basin is unable to garden the "later-formed" Serenitatis melt. Therefore, given the general sequence of lunar basins, especially those formed during the mid- to late- period, the distribution of basin melt in the near surface would not be significantly changed but the melt abundance of early-formed basins surrounding the later-formed basins might be altered.

4.4 Other notable uncertainties in the model's prediction of the distribution of basin melt

The transient cavity sizes of basins are not well constrained, the estimates being diverse (Hikida & Wieczorek 2007; Miljković et al. 2016; Potter, Kring, et al. 2012; Potts & von Frese 2003). For example, the D_t of Imbrium basin has been estimated to be 744 km (Wieczorek & Phillips 1999) and 895 km (Hikida & Wieczorek 2007). However, although it would change the absolute abundances, the structure of the distribution of basin melt would not be changed (Liu et al. 2019).

In addition, the early Moon, during which time most basins were formed, is thought to have been much hotter than at later times (Laneuville et al. 2013). The higher internal energy leads to higher melt production since a warmer target requires less energy to melt (Zhu et al. 2017). The distribution of melt in the ejecta is also affected by the thermal state of the Moon. For a warmer target, Zhu et al. (2017) found that in a basin-forming impact, the melt fraction in ejecta material is almost constant with distance at ~20%. Therefore, on the younger Moon there might be more basin melt near the surface leading to probably even more prominent abundance of these old basin melt in the near-surface (Liu et al. 2019). In addition, for the largest SPA basins, some ejecta may be lost close to five radii because of the high launch velocity.

The efficiency of melt diffusion is significantly influenced by the degree of mixing with local material during ejecta emplacement. As seen from Figure 3d-f, without the consideration of this mixing process, the Imbrium melt in the near-surface would be much more abundant. In the western part of the Crisium basin, melt abundance would be reduced due to the coverage by Imbrium ejecta. The fraction of remaining Serenitatis melt would strongly decrease because of the coverage by both Crisium and Imbrium ejecta. Nevertheless, quantitative investigation of the entrainment of local material by ejecta needs to be further studied (Hörz et al. 1983; Zhu & Wünnemann 2013).

Impacts forming craters smaller than 5 km in radii are not taken into account in this model. We expect that the gardening by these smaller impacts would reset the age of a component of the material and mix it to a more homogeneous state. We expect the older basin-derived components to remain essentially the same, minus this younger component.

Furthermore, our model did not take into account distal regions beyond five radii. Such processes lead to regional, melt-enriched areas (Hubbard et al. 1971). However, these processes are more sporadic and the volume is small. In addition, most impacts on the Moon occur with an oblique incidence angle. While resulting craters remain mostly near-circular (except for very shallow impact angles), the ejecta distribution can deviate more strongly from concentric symmetry: the ejecta of small craters are asymmetric only at distances where continuous ejecta blankets do not exist whereas the ejecta of large basins are asymmetric even near the crater rim (Shuvalov 2011). Given the large number of the smaller impacts, the asymmetry distribution of ejecta will be averaged out, but the oblique impact angle may significantly affect the ejecta distribution of certain basins.

The formation process of the SPA basin is still not fully understood. The large melt volume, resulting from the higher internal energy, may have led to the formation of a deep and broad melt pool within the basin (Potter, Collins, et al. 2012). Our model may underestimate the global distribution of SPA melt, but SPA melt in the near surface should still be predominant on average (but not at landing sites close to Imbrium). However, melts with ages of 4.3 Ga are rare among landing site samples and possible reasons have been identified in the previous discussion. The lack of evidence for SPA melt could imply that there may have been more old basin-forming events that have not been identified.

5 Conclusion

The formation time of lunar basins, is crucial for the study of late accretion in the inner solar system. To quantitatively understand the spatial diffusion of basin- and crater-derived impact melt, we developed a numerical model to simulate the long-term impact gardening process for a given impact flux scenario. The abundance and presence of impact melt with different ages, both globally and at specific Apollo and Luna sampling sites, were estimated and compared with K-Ar age distributions of impact melt breccias. Combined with the spatial distribution of basins, the probable distribution of basin-derived impact melt was discussed.

On a global basis, the estimated melt component in the near-surface shows, not unexpectedly, that impact melt from the SPA basin should be highly abundant. But very few melt rocks with isotopic ages of 4.3 Ga have been found among lunar samples. Imbrium-derived melt is also dominant in the near surface due to its late formation time and large size and here model and isotopic ages tend to match. Impact melt generated by the other basins was subject to cumulative gardening and thus the remainder in the near surface was significantly diluted, although melt from these basins is still quite abundant at depth. Older basin melt, especially from basins before 3.8 Ga, may have survived in the lunar meteorites, but the expected small fragments, resulting from long-term pulverization, make it difficult to investigate such impact melt clasts. In contrast, because of the low impact rate during the last 3 Ga, the melt of smaller impacts is more easily preserved and the clasts may still be intact, making the occurrence of young impactites more likely among lunar meteorites.

The estimated melt abundances at the Apollo 14-17 and Luna 20 sampling sites suggests that the regional impact melt component is closely related to the nearby basins (and occasionally nearby craters). Most of the collected samples at the Apollo 14-17 sites are likely to have been mixed with Imbrium melt, as suggested by previous radioisotope dating and geochemical studies. The model predicts that the modelled melt with an apparent model age of 3.87 Ga (based on the Neukum, 1983, chronology function), which appears to correspond to Pb-Pb phosphate ages of ~3.9 Ga (Snape et al. 2016), is almost all derived from the Imbrium basin. This result suggests that the K-Ar ages of impact melt breccias near 3.9 Ga in Apollo 14-17 samples represent the mixing of Imbrium melt with un-heated ejecta. In addition, the simulation results indicate that the formation time of Crisium basin could be close to Imbrium basin with the age of ~3.9 Ga as suggested by Stöffler (2006), and the impact melt of ~3.9 Ga in the Apollo 17 samples could be a mixture of both Imbrium and Crisium ejecta. The Luna 20 sampling site is close to the Crisium basin. We estimated the fraction of Crisium melt in the melt of 4.07 Ga (the CSFD model age of Crisium basin; or ~3.9 Ga, assuming the radioisotope age is correct) to be ~0.9.

All the Apollo 14-17 and Luna 20 samples should contain components of Serenitatis melt, but may not be mixed with the ejecta of the youngest Orientale basin. The melt of older surrounding basins, including SPA melt, also should occur, however, the content has been diluted by gardening. The Apollo 14, 16, 17 samples may also contain Humorum, Nectaris and Smythii melt, respectively. Little other basin-sourced melt is expected in the Apollo 15 samples than Imbrium, Serenitatis and SPA melt, however, only Imbrian K-Ar ages do occur. Luna 20 samples may contain Smythii and Nectaris melt. Other peaks observed in the K-Ar age distributions more likely derive from smaller-scale impact events or reflect disturbed Ar-Ar systematics.

Acknowledgments: We acknowledge discussions about cratering processes and formation of impact melt with Menghua Zhu, Lukas Manske, and Robert Luther. We thank Wilhelm Zuschneid for proof-reading and many helpful suggestions. This work was supported by German Research Foundation (DFG) CRC TRR 170, subproject A4. This is TRR 170 contribution 82.

References

Cassata, W.S., Renne, P.R. & Shuster, D.L., 2009. Argon diffusion in plagioclase and implications for thermochronometry: A case study from the Bushveld Complex, South Africa. *Geochimica et Cosmochimica Acta*, 73(21), pp.6600–6612.

Chapman, C.R., Cohen, B.A. & Grinspoon, D.H., 2007. What are the real constraints on the existence and magnitude of the late heavy bombardment? *Icarus*, 189(1), pp.233–245.

Cintala, M.J. & Grieve, R.A.F., 1998. Scaling impact melting and crater dimensions: Implications for the lunar cratering record. *Meteoritics and Planetary Science*, 33(4), pp.889–912.

Cohen, B.A., 2000. Support for the Lunar Cataclysm Hypothesis from Lunar Meteorite Impact Melt Ages. *Science*, 290(5497), pp.1754–1756.

Fassett, C.I. et al., 2012. Lunar impact basins: Stratigraphy, sequence and ages from superposed impact crater populations measured from Lunar Orbiter Laser Altimeter (LOLA) data. *Journal of Geophysical Research: Planets*, 117(2), pp.1–13.

Fernandes, V.A. et al., 2013. The bombardment history of the Moon as recorded by 40 Ar-39 Ar chronology. *Meteoritics and Planetary Science*, 48(2), pp.241–269.

Gomes, R. et al., 2005. Origin of the cataclysmic Late Heavy Bombardment period of the terrestrial planets. *Nature*, 435, p.466.

Grange, M.L., Nemchin, A.A. & Jourdan, F., 2010. Review of Ages of Lunar Impact Rocks: Implication to the Timing of Serenitatis and Imbrium Impacts and the LHB Model. In *Lunar and Planetary Science Conference*. Lunar and Planetary Science Conference. p. 1275.

Hartmann, W., 1995. Planetary cratering I: Lunar highlands and tests of hypotheses on crater populations. *Meteoritics*, 30, p.451.

Hartmann, W.K., 1975. Lunar "cataclysm": A misconception? *Icarus*, 24(2), pp.181–187.

Hiesinger, H. and Head III, J.W., 2006. New views of lunar geoscience: An introduction and overview. Reviews in mineralogy and geochemistry, 60(1), pp.1-81.

Hikida, H. & Wieczorek, M.A., 2007. Crustal thickness of the Moon: New constraints from gravity inversions using polyhedral shape models. *Icarus*, 192(1), pp.150–166.

Hörz, F., Ostertag, R. & Rainey, D.A., 1983. Bunte Breccia of the Ries: Continuous deposits of large impact craters. *Reviews of Geophysics*, 21(8), pp.1667–1725.

Hubbard, N.J. et al., 1971. The composition and derivation of Apollo 12 soils. *Earth and Planetary Science Letters*, 10(3), pp.341–350.

Jourdan, F., Renne, P.R. & Reimold, W.U., 2009. An appraisal of the ages of terrestrial impact structures. *Earth and Planetary Science Letters*, 286(1), pp.1–13.

Jourdan, F., 2012. The 40Ar/39Ar dating technique applied to planetary sciences and terrestrial impacts. Australian Journal of Earth Sciences, 59(2), pp.199-224.

Korotev, R.L., 1994. Compositional variation in Apollo 16 impact-melt breccias and inferences for the geology and bombardment history of the Central Highlands of the Moon. *Geochimica et Cosmochimica Acta*, 58(18), pp.3931–3969.

Laneuville, M. et al., 2013. Asymmetric thermal evolution of the Moon. *Journal of Geophysical Research: Planets*, 118(7), pp.1435–1452.

Liu, T. et al., 2019. Regolith mixing by impacts : Lateral diffusion of basin melt. *Icarus*, 321(0019-1035), pp.691–704.

McKinnon, W.B. et al., 1997. Cratering on Venus: Models and Observations. In *Venus II: Geology, Geophysics, Atmosphere, and Solar Wind Environment*. p. 969.

Melosh, H.J., 1989. *Impact cratering: A geologic process*, New York: Oxford University.

Michael, G., Basilevsky, A. & Neukum, G., 2018. On the history of the early meteoritic bombardment of the Moon: Was there a terminal lunar cataclysm? *Icarus*, 302, pp.80–103.

Miljković, K. et al., 2016. Subsurface morphology and scaling of lunar impact basins. *Journal of Geophysical Research: Planets*, 121(9), pp.1695–1712.

Morbidelli, A. et al., 2012. A sawtooth-like timeline for the first billion years of lunar bombardment. *Earth and Planetary Science Letters*, 355–356, pp.144–151.

Naumenko-Dèzes, M.O., Nägler, T.F., Mezger, K. and Villa, I.M., 2018. Constraining the 40K decay constant with 87Rb-87Sr–40K-40Ca chronometer intercomparison. Geochimica et cosmochimica acta, 220, pp.235-247.

Neukum, G., 1983. Meteoritenbombardement und Datierung Planetarer Oberflaechen. *Habilitation Dissertation for Faculty Membership, Univ. of Munich*, pp.1–186.

Neumann, G.A. et al., 2015. Lunar impact basins revealed by Gravity Recovery and Interior Laboratory measurements. *Science Advances*, 1(9).

Niihara, T., Beard, S.P., Swindle, T.D., Schaffer, L.A., Miyamoto, H. and Kring, D.A., 2019. Evidence for multiple 4.0–3.7 Ga impact events within the Apollo 16 collection. Meteoritics & Planetary Science, 54(4), pp.675-698.Norman, M.D. et al., 2016. Crystal accumulation in a 4.2 Ga lunar impact melt. *Geochimica et Cosmochimica Acta*, 172, pp.410–429.

Norman, M.D., Duncan, R.A. & Huard, J.J., 2006. Identifying impact events within the lunar cataclysm from 40Ar–39Ar ages and compositions of Apollo 16 impact melt rocks. *Geochimica et Cosmochimica Acta*, 70(24), pp.6032–6049.

Norman, M.D., Duncan, R.A. & Huard, J.J., 2010. Imbrium provenance for the Apollo 16 Descartes terrain: Argon ages and geochemistry of lunar breccias 67016 and 67455. *Geochimica et Cosmochimica Acta*, 74(2), pp.763–783.

Norman, M.D. & Nemchin, A.A., 2014. A 4.2 billion year old impact basin on the Moon: U–Pb dating of zirconolite and apatite in lunar melt rock 67955. *Earth and Planetary Science Letters*, 388, pp.387–398.

Oberbeck, V.R. et al., 1975. On the origin of the lunar smooth plains. *The Moon*, 12(1), pp.19–54.

Orgel, C. et al., 2018. Ancient Bombardment of the Inner Solar System: Reinvestigation of the "Fingerprints" of Different Impactor Populations on the Lunar Surface. *Journal of Geophysical Research: Planets*, 123(3), pp.748–762.

Petro, N.E. & Pieters, C.M., 2006. Modeling the provenance of the Apollo 16 regolith. *Journal of Geophysical Research*, 111(E9), p.E09005.

Potter, R.W.K., Collins, G.S., et al., 2012. Constraining the size of the South Pole-Aitken basin impact. *Icarus*, 220(2), pp.730–743.

Potter, R.W.K., Kring, D.A., et al., 2012. Estimating transient crater size using the crustal annular bulge: Insights from numerical modeling of lunar basin-scale impacts. *Geophysical Research Letters*, 39(18), pp.1–5.

Potts, L. V & von Frese, R.R.B., 2003. Comprehensive mass modeling of the Moon from spectrally correlated free-air and terrain gravity data. *Journal of Geophysical Research*, 108(E4), p.5024.

Riedel, C. et al., 2018. A New Tool to Account for Crater Obliteration Effects in Crater Size-Frequency Distribution Measurements. *Earth and Space Science*, 5(6), pp.258–267.

Robinson, M.S. et al., 2010. Lunar reconnaissance orbiter camera (LROC) instrument overview. *Space Science Reviews*, 150(1–4), pp.81–124.

Rotenberg, E., Davis, D.W., Amelin, Y., Ghosh, S. and Bergquist, B.A., 2012. Determination of the decay-constant of 87Rb by laboratory accumulation of 87Sr. Geochimica et Cosmochimica Acta, 85, pp.41-57.

Ryder, G., Spudis, P.D. & Taylor, G.J., 1989. The case for planetary sample return missions: Origin and evolution of the Moon and its environment. *Eos, Transactions American Geophysical Union*, 70(47), pp.1495–1509.

Schärer, U., 1998. Dating of Impact Events. In D. Benest & C. Froeschlé, eds. *Impacts on Earth*. Berlin, Heidelberg: Springer Berlin Heidelberg, pp. 157–183.

Schultz, P.H. & Gault, D.E., 1985. Clustered impacts: Experiments and implications. *Journal of Geophysical Research*, 90(B5), p.3701.

Shervais, J.W., Taylor, L.A. & Lindstrom, M.M., 1985. Apollo 14 Mare basalts: Petrology and geochemistry of clasts from Consortium Breccia 14321. *Journal of Geophysical Research: Solid Earth*, 90(S02), pp.C375–C395.

Shuvalov, V., 2011. Ejecta deposition after oblique impacts : An influence of impact scale. *Meteoritics & Planetary Science*, 1718(11), pp.1713–1718.

Snape, J.F. et al., 2016. Phosphate ages in Apollo 14 breccias: Resolving multiple impact events with high precision U–Pb SIMS analyses. *Geochimica et Cosmochimica Acta*, 174, pp.13–29.

Spudis, P.D., Wilhelms, D.E. & Robinson, M.S., 2011. The Sculptured Hills of the Taurus Highlands: Implications for the relative age of Serenitatis, basin chronologies and the cratering history of the Moon. *Journal of Geophysical Research*, 116(12), p.E00H03.

Stöffler, D., 2006. Cratering history and lunar chronology. *Reviews in Mineralogy and Geochemistry*, 60(1), pp.519–596.

Tera, F., Papanastassiou, D.A. & Wasserburg, G.J., 1974. Isotopic evidence for a terminal lunar cataclysm. *Earth and Planetary Science Letters*, 22(1), pp.1–21.

Wieczorek, M.A. & Phillips, R.J., 1999. Lunar Multiring Basins and the Cratering Process. *Icarus*, 139, pp.246–259.

Zellner, N.E.B., 2017. Cataclysm no more: New views on the timing and delivery of lunar impactors. *Origins of Life and Evolution of Biospheres*, 47(3), pp.261–280.

Zhu, M.-H. et al., 2019. Reconstructing the late-accretion history of the Moon. *Nature*, 571(7764), pp.226–229.

Zhu, M.-H. & Wünnemann, K., 2013. Modeling of Meteorite Impact-Induced Secondary Mass Wasting {\mdash} Case Study by Means of the Bunte Breccia Ejecta Blanket at Ries Crater, Germany. In *Lunar and Planetary Science Conference*. Lunar and Planetary Science Conference. p. 1921.

Zhu, M.-H., Wünnemann, K. & Artemieva, N., 2017. Effects of Moon’s thermal state on the impact basin ejecta distribution. *Geophysical Research Letters*, 44(22), p.11,211-292,300.